Electronic surface excitations of cavities in metals

Ll. Serra and F. Garcías
Departament de Física, Universitat de les Illes Balears, E-07071 Palma de Mallorca, Spain

J. Navarro
Departament de Física Atòmica, Molecular i Nuclear, Universitat de València, E-46100 Burjassot, València, Spain

N. Barberán, M. Barranco, and M. Pi
Departament d'Estructura i Constituents de la Matèria, Facultat de Física, E-08028 Barcelona, Spain
(Received 14 October 1991; revised manuscript received 24 April 1992)

Within the random-phase approximation (RPA), we have obtained the average surface-plasmon energy of voids and bubbles in nearly-free-electron metals using energy-weighted moments of the electronic response to operators of type $r^{-(L+1)}Y_{L0}$. We have used a local-density approximation of Slater and Wigner type for the exchange and correlation energies, respectively, and the jellium model for the positive ionic background. Compact expressions for the plasmon average energies are given, which allow one to discuss clearly the role played by the kinetic- and Coulomb energy contributions to the restoring force of the L modes. The effect of the electronic surface diffuseness is clarified. For the numerical applications, we have used an improved Thomas-Fermi-Weizsäcker model already employed in similar studies on metal spheres. Using this model, we have also studied the static polarizability of voids. In the case of bubbles, the gas filling the cavity is modeled by a constant dielectric function whose effect is incorporated in the calculation of the electronic density *and* in the RPA response. A comparison with the experimental data is presented.

I. INTRODUCTION

Voids are produced inside irradiated metals under certain conditions of temperature and irradiation dose.[1] Apart from its intrinsic scientific interest in the study of microstructures, the understanding of the electronic structure of cavities in metals and of their excitations is of some technological importance in the study of swelling and deterioration of materials exposed to neutron and heavy-ion irradiation in the core of fast reactors.

Metal irradiation produces rare-gas impurities either by nuclear reaction or by ion implantation. These impurities are essentially insoluble[2] and tend to precipitate to form bubbles, i.e., voids filled with gas usually overpressurized with respect to the thermal equilibrium value.[3]

The existence of bubbles was first confirmed experimentally by Henoc and Henry[4] (theoretical predictions were available before, see Refs. 5 and 6), and since then many experimental and theoretical investigations on the properties of spherical defects and bubbles in metals have been reported (see Refs. 7–14, for example, and references therein).

The solution of the Laplace equation corresponding to a sharp-surface spherical void surrounded by a metal modeled by the Drude dielectric constant, yields the classical dispersion relation for the L mode[5]

$$\omega_{\rm cl}^2 = \omega_p^2 \frac{L+1}{2L+1} , \tag{1}$$

where $\omega_{\rm cl}$ is the frequency of a surface mode carrying an angular momentum L, and ω_p is the plasma frequency.

Equation (1) is the model-independent large void limit for all nonretarded dispersion relation calculations. An extension of the sharp-surface electrostatic model to include spatial dispersion exists[10] which produces results within a random-phase approximation (RPA). Aers, Paranjape, and Boardman[11] have included spatial dispersion within the hydrodynamical model through a pressure term, retardation effects, and an improved electronic profile that goes beyond the sharp-surface model. More recently, a truncated ("long-wavelength") version of the RPA was used by Wu and Beck[13] to study the $L = 1$ and 2 surface modes of a void. They have found a size-dependent plasma frequency which is gradually blueshifted as the radius of the cavity decreases.

For high enough implantation doses, regular arrays of bubbles have been observed[12,14] which can be made of several thousands of bubbles. In his work on void clusters,[7] Lucas has used a local dielectric constant for a metallic matrix containing a regular array of identical voids, and has studied the band structure of the monopole ($L = 0$) plasmon mode.

In the present work, we want to address the surface collective excitations of a bubble using a RPA sum-rules approach which has proved to be useful in previous studies on metallic spheres.[15–20] To allow for a sensible comparison of our results with the experimental data, we incorporate into the formalism two dielectric constants that, in the more general case, model the gas inside the bubble and the positive ionic background in the metal, respectively. We represent the neutralizing positive background surrounding the void by a jellium and assume the

density of cavities to be small enough in order to consider only a single void in a large metal volume. We assume that the void radius is small compared to the characteristic wavelength $\lambda_p = 2\pi c/\omega_p$ (about 1500 a.u. for Al, which has $\omega_p = 0.58$ a.u.), so that retardation effects may be neglected.

This paper is organized as follows. In Sec. II we briefly recall the RPA sum-rules method and present the main analytical results of our work for voids and bubbles. In Sec. III we calculate the electronic structure of these objects using an improved Thomas-Fermi-Weizsäcker (ITFW) model, and apply it to obtain the static dipole polarizability of a void. We present the numerical results for the surface plasmon in Sec. IV, as well as a comparison with some available experimental data. The conclusions are drawn in Sec. V, and the general expression of the Coulomb interaction between two elementary charges used in Secs. II and IV is given in the Appendix.

II. RPA SUM RULES

A. General description

RPA sum rules (SR) have been already used in the description of collective excitations of nearly-free-electron (NFE) metals.[15–21] To avoid unnecessary repetitions, we refer the reader to these references, and references therein, for a detailed account of the method. We simply want to recall here that the SR contain information about the excitation modes of the system through an energy-weighted average of the strength function $S(E)$ defined as

$$S(E) = \sum_n \delta(E - E_n)\ |\langle n|Q|0\rangle|^2 \ , \tag{2}$$

where Q is the external operator representing the field that excites the system and E_n, $|n\rangle$, and $|0\rangle$ are the excitation energies, excited states, and ground state (g.s.) of the system, respectively. The sum rule m_k is defined as the kth-energy moment of $S(E)$,

$$m_k = \int E^k\, S(E)\, dE = \sum_n E_n^k |\langle n|Q|0\rangle|^2 \ . \tag{3}$$

The physical interest of these moments stems from the fact that, if the system has states of strong collective nature and if the operator Q is chosen so that it does not simultaneously excite different normal modes, then the strength function $S(E)$ is concentrated in a narrow region and the knowledge of a few m_k furnishes useful information about that state, avoiding on one hand the much more cumbersome task of fully evaluating $S(E)$, and yielding on the other hand compact formulas that can be used to estimate the energy and width of the collective mode.

From a practical point of view, the most useful SR are the m_{-1}, m_1, and m_3 ones. This is so because they can be obtained with RPA accuracy by much simpler Kohn-Sham (KS) calculations. From these SR, we can define two average energies,

$$E_3 = (m_3/m_1)^{1/2} \ , \qquad E_1 = (m_1/m_{-1})^{1/2} \ , \tag{4}$$

which are, respectively, upper and lower bounds to the average energy $\bar{E} \equiv m_1/m_0$, $E_1 \le \bar{E} \le E_3$, and can be employed to estimate the $S(E)$ variance $\sigma^2 \le (E_3^2 - E_1^2)/4$. E_1 is closely related to the hydrodynamical (long-wavelength) response of the system, whereas E_3 can be associated with its "elastic" (short-wavelength), collisionless regime response (see Ref. 21 and references therein). For the present purposes, we shall be mainly concerned with E_3 which bears the relevant physical information, as plasma oscillations usually take place in a collisionless regime. Nevertheless, for the sake of completeness we will also present some results for E_1.

We have chosen as external field Q the one-electron operator corresponding to the irregular solution at the origin of the Laplace equation, i.e.,

$$Q(\mathbf{r}) = r^{-(L+1)} Y_{L0} \ , \tag{5}$$

where Y_{L0} is a spherical harmonic. This choice supposes that the electronic density is zero at the center of the void. Consequently, only voids whose density is negligible within a volume around the origin can be studied following this method. We shall come back to this point in Sec. IV.

To describe the electron structure, we have used a density functional $\varepsilon[n(\mathbf{r})]$ consisting of a kinetic term (T), an electron-electron (e-e) Coulomb direct term, a Coulomb exchange term of Slater type,

$$\varepsilon_{\rm ex} = -\frac{3}{4}\left(\frac{3}{\pi}\right)^{1/3} n(r)^{4/3} \equiv -c_x\, n(r)^{4/3} \ , \tag{6}$$

a correlation term of Wigner type,

$$\varepsilon_{\rm cor} = -\frac{a\, n(r)}{b + [3/4\pi n(r)]^{1/3}} \ , \tag{7}$$

where $a = 0.44$ a.u. and $b = 7.8$ a.u. (we shall use atomic units throughout), and a jellium-jellium (j-j) plus a jellium-electron (j-e) Coulomb contribution.

B. The m_1 and m_3 sum rules for a void

It is very simple to obtain m_1 for the operator Q of Eq. (5). Following the method outlined in Refs. 17–19, we get

$$m_1 = \tfrac{1}{2}(2L+1)(L+1) \int_0^\infty dr\, \frac{n(r)}{r^{2L+2}} \ , \tag{8}$$

where $n(r)$ is the g.s. (spherically symmetric) electronic density.

The calculation of m_3 is straightforward. Due to the fact that $\Delta Q = 0$, m_3 has no explicit contributions from terms like ε_{ex} and ε_{cor} which only depend on the electronic density.[19] After a lengthy calculation, one gets

$$m_3 = m_3(T) + m_3(C) \ , \tag{9}$$

where the Coulomb contribution $m_3(C)$ containing the e-e and j-e contributions is given by

$$m_3(C) = (L+1)^2 \left[(L+2) \int_0^\infty dr \, \frac{n(r)}{r^{2L+5}} \int_0^r 4\pi r_1^2 \, dr_1 \, [n(r_1) - n_J(r_1)] + 2\pi \int_0^\infty dr \, \frac{n(r) n_J(r)}{r^{2L+2}} \right] \ . \tag{10}$$

The jellium density $n_J(r)$ of a void of radius R is defined by means of a unit step function

$$n_J(r) = n_0 \, \theta(r - R) \ , \tag{11}$$

where $n_0 = 3/(4\pi r_s^3)$, r_s being the bulk radius per electron.

The kinetic term $m_3(T)$ is given by

$$m_3(T) = \tfrac{1}{4}(L+1)(L+2)(2L+1) \int_0^\infty \frac{dr}{r^{2L+4}} \left[-\frac{L+3}{3}(2\tau - 3\lambda) + \tfrac{4}{3}(2L+3)\tau \right] \ . \tag{12}$$

In this expression, $\tau(r)$ is the kinetic-energy density defined as

$$T \equiv \tfrac{1}{2} \int d^3r \, \tau(r) \equiv \tfrac{1}{2} \int d^3r \sum_i |\nabla \varphi_i(\mathbf{r})|^2 \ , \tag{13}$$

where $\varphi_i(\mathbf{r})$ is the ith single-electron wave function. The function $\lambda(r)$ is a kind of centrifugal kinetic-energy density.[17,18] If one uses the Thomas-Fermi approximation to evaluate Eq. (12), this formula is simplified by the fact that $2\tau = 3\lambda$.[22] Since this equality approximately holds in the general case, we shall neglect the contribution of the first term in the right-hand side (rhs) of Eq. (12) in all the numerical applications.

We would like to stress that the m_1 and m_3 expressions depend only on the KS particle and kinetic-energy densities of the unperturbed system (this advantage is also shared with the truncated RPA method of Ref. 13), and that both SR can be obtained with RPA precision by numerical quadratures.

Once the SR expressions have been worked out, different approximations for the electronic structure can be employed in order to obtain approximate analytical formulas. Indeed, it is quite instructive to carry out the integrals in Eqs. (8), (10), and (12) for a step electronic density which is one of the most often used in the literature.[6,8,15,20] In this case, $\tau = \frac{3}{5}(3\pi^2)^{2/3} n_0^{5/3} \equiv \tau_0$ and one gets

$$m_1 = \frac{1}{2} \frac{L+1}{R^{2L+1}} n_0 \ , \tag{14}$$

$$m_3(C) = \frac{2\pi n_0^2}{R^{2L+1}} \frac{(L+1)^2}{2L+1} \ , \tag{15}$$

$$m_3(T) = \tfrac{1}{3}(L+1)(L+2)(2L+1) \frac{\tau_0}{R^{2L+3}} \ . \tag{16}$$

Thus,

$$E_3^2 = \tfrac{2}{3}(L+2)(2L+1) \frac{\beta_F^2}{R^2} + \omega_p^2 \frac{L+1}{2L+1} \ , \tag{17}$$

where $\omega_p = (4\pi n_0)^{1/2}$ is the plasma frequency and $\beta_F = (\frac{3}{5})^{1/2} v_F$, v_F being the Fermi velocity.

In spite of the crude step density model we have used for $n(r)$ (the inclusion of the kinetic energy in whatever approximation leads to a spill-in), Eq. (17) constitutes an interesting result of the present study. It shows in a transparent way how finite-size effects come about. We will show in Sec. IV how the electron surface diffuseness modifies this result. Notice that when R goes to infinity, Eq. (17) yields the classical limit, Eq. (1).

Finally, we would like to draw attention to an application of m_1 that has been often overlooked in the use of the RPA method for describing the electronic excitations of NFE metals (see, however, Ref. 23). Starting from Eq. (3), it can be easily shown that

$$m_1 = \tfrac{1}{2} \langle 0 | [Q, [H, Q]] | 0 \rangle = \tfrac{1}{2} \int d^3r \, (\nabla Q)^2 \, n(r) \ , \tag{18}$$

where H is the Hamiltonian of the electron system. As m_1 can be calculated either from Eq. (3) using the RPA $S(E)$ function or from Eq. (18) using for $n(r)$ the KS g.s. density, it provides a test on the numerical accuracy in evaluating $S(E)$, which sometimes is not easy to ascertain. In the particular case of the dipole mode of a metal sphere, a test is provided by Sorbello's electrostatic force rule,[24] widely used in that case (see, for example, Refs. 25–27). However, the force rule cannot be used in more general situations, like for q-dependent operators[19] and/or multipolarities higher than $L = 1$ (Refs. 17 and 18), or in the present case, whereas the test on m_1 is of general applicability.

C. The case of a void filled with dielectric (bubble)

As we have indicated in the Introduction, to compare the results of the calculations with available experimental data, one has to incorporate in the formalism the response properties of the gas that appears inside the ex-

perimentally studied bubbles. Its presence changes the values of the plasmon energies in two different ways. One is through the modification it induces in the g.s. electronic structure at the void surface. This is an implicit way that shows up as a self-consistency effect: the diffuseness of the g.s. density and the electronic "spill-in" increase because the dielectric inside the cavity screens the *e-e* interaction. As a consequence, the average electronic density at the void surface tends to decrease. The other effect of the dielectric is what we shall call an explicit effect, in the sense that the dielectric constant explicitly appears in the formulas of the plasmon frequency. We shall show that this second effect is, by far, the most important one.

We assume constant dielectric functions to model the gas filling the bubble (ϵ_1) as well as the *ionic* background in the metal (ϵ_2). This assumption is valid when the energy values of the plasmon excitations are far from those of the inner-shell excitations of the dielectrics, which is not always the case. As a further approximation, we have only modified the Coulomb direct term in the presence of dielectrics, but not the exchange or correlation terms (a similar procedure was used in Ref. 28 to study the electronic polarizability of small metal spheres embedded in a dielectric). This procedure is in part justified by the fact that $\varepsilon_{\rm ex}$ and $\varepsilon_{\rm cor}$ have lesser influence on the g.s. $n(r)$ and $\tau(r)$ than the other terms in the density functional, and that the electronic response is mainly determined by the Coulomb direct interaction.[13,23]

To calculate $m_3(C)$ in the case of two regions of different dielectric constants, one has first to obtain the expression of the corresponding scalar Coulomb potential $\Phi(\mathbf{r}_1,\mathbf{r}_2)$. This is given in the Appendix for two elementary charges at $\mathbf{r}_1$ and $\mathbf{r}_2$ in a space occupied by a spherical dielectric of radius R and constant ϵ_1 surrounded by an infinite dielectric of constant ϵ_2. Using that expression, the total Coulomb direct energy for an arbitrary charge density $\rho(\mathbf{r})$ reads

$$E_C = \tfrac{1}{2}\iint d^3r_1\, d^3r_2\, \rho(\mathbf{r}_1)\,\Phi(\mathbf{r}_1,\mathbf{r}_2)\,\rho(\mathbf{r}_2)\ . \tag{19}$$

Starting from Eq. (19) and using the method of Refs. 18 and 19, a rather cumbersome calculation yields

$$\begin{aligned} m_3(C) = 2\pi(L+1)^2 \Bigg[& \frac{1}{\epsilon_2}\int_R^\infty dr\,\frac{n(r)\,n_J}{r^{2L+2}} + \frac{\epsilon_2-\epsilon_1}{\epsilon_2}\frac{L(2L+1)R^{2L+1}}{\epsilon_1 L+\epsilon_2(L+1)}\left(\int_R^\infty dr\,\frac{n(r)}{r^{2L+2}}\right)^2 \\ & + \left(\frac{1}{\epsilon_1}-\frac{1}{\epsilon_2}\right)\frac{n(R)}{R^{2L+4}}\int_0^R dr\,r^2 n(r) + \frac{2(L+2)}{\epsilon_1}\int_0^R dr_1\,\frac{n(r_1)}{r_1^{2L+5}}\int_0^{r_1} dr\,r^2\,n(r) \\ & - \frac{2(L+2)}{\epsilon_2}\int_R^\infty dr_1\,\frac{n(r_1)}{r_1^{2L+5}}\int_0^{r_1} dr\,r^2\,n_{\rm net}(r)\Bigg]\ , \end{aligned} \tag{20}$$

where $n_{\rm net}(r) \equiv n_J(r) - n(r)$. Adding to Eq. (20) $m_3(T)$ given by Eq. (12), one gets m_3 in the case of a bubble.

Again, it is interesting to evaluate Eq. (20) for an electronic step density. In this case, the last three terms in Eq. (20) are zero and one gets

$$m_3(C) = \frac{2\pi n_0^2}{R^{2L+1}}\,\frac{(L+1)^2}{\epsilon_1 L+\epsilon_2(L+1)}\ . \tag{21}$$

Thus,

$$E_3^2 = \tfrac{2}{3}(L+2)(2L+1)\frac{\beta_F^2}{R^2} + \omega_p^2\,\frac{L+1}{\epsilon_1 L+\epsilon_2(L+1)}\ , \tag{22}$$

which is analogous to Eq. (17).

To conclude this section, we would like to stress again the simplicity of formulas (8), (12), and (10) or (20) that allow us to obtain the m_1 and m_3 SR (thus an average frequency of the surface modes within RPA) from g.s. quantities obtained in the KS approximation. Moreover, the fact that they only depend on the unperturbed electron and kinetic-energy densities offers the interesting possibility of evaluating E_3 employing a semiclassical method, like the ITFW model of Refs. 18, 19, and 26.

III. THE IMPROVED THOMAS-FERMI-WEIZSÄCKER APPROXIMATION

A. Electronic structure

The problem of the electronic structure of vacancies in metals has been addressed by Manninen *et al.*[29] in the KS and Thomas-Fermi-Weizsäcker approximations. Wu and Beck[13] have described voids using a single- or double-step potential to generate the single-electron wave functions. However, as their calculations are for voids whose size is similar to ours, we shall use their results to test our electronic densities.

What we shall call ITFW approximation consists in using as kinetic-energy density $\tau(r)$ the following expression:

$$\tau(r) = \gamma\, n^{5/3}(r) + \frac{\beta}{4}\,\frac{[\nabla n(r)]^2}{n(r)}\ , \tag{23}$$

where $\gamma \equiv \frac{3}{5}(3\pi^2)^{2/3}$ and $\beta = \frac{2}{9}$. The latter value is heuristic and has been fixed to reproduce the densities obtained in Ref. 13 (see below). The use of the value $\beta = \frac{1}{9}$ deduced by Kirzhnits[30] results in too steep densities as compared with the quantal ones (see Ref. 31 and

references therein). From previous studies of collective excitations in metal clusters,[18,26,32] a value bigger than $\frac{1}{9}$ yields results in better agreement with the KS results than the original value of Kirzhnits. To obtain the g.s. ITFW density, one has to solve the Euler-Lagrange (EL) equation,

$$\frac{\delta\varepsilon[n]}{\delta n} = \mu \ , \tag{24}$$

where μ is the electron chemical potential, and $\varepsilon[n]$ consists of the ε_{ex} and ε_{cor} pieces defined in Eqs. (6) and (7), of the ITFW kinetic energy per unit volume $\varepsilon_{kin} = \tau(r)/2$, and of the usual Coulomb direct (e-e, j-e, and j-j) energy terms.

Equation (24) has been solved using the method of Ref. 31 within a large sphere of radius R_∞, typically of the order of $R + 20$ a.u., in which we have imposed charge neutrality. The boundary conditions on $n(r)$ are $n'(0) = n'(R_\infty) = 0$. To obtain the Coulomb direct potential $\phi(r)$ entering Eq. (24), we have solved the Poisson equation

$$\Delta\phi(r) = \begin{cases} -\dfrac{4\pi}{\epsilon_1} n_{net}(r) & \text{for } r < R \\ -\dfrac{4\pi}{\epsilon_2} n_{net}(r) & \text{for } r > R \ , \end{cases} \tag{25}$$

imposing the matching condition

$$\left[\epsilon_1 \frac{\partial\phi}{\partial r}\right]^{in}_{r=R} = \left[\epsilon_2 \frac{\partial\phi}{\partial r}\right]^{out}_{r=R} \ , \tag{26}$$

at the bubble edge, as well as the conditions $(r\phi)_{r=0} = (r\phi)_{R_\infty} = 0$, the latter one due to charge neutrality. $n_{net}(r)$ is defined after Eq. (20). As a test on the numerical accuracy, we have checked that $n(R_\infty) = n_0$, Eq. (11), and that μ is r independent and coincides with the bulk value μ_0 obtained from Eq. (24) after dropping all the gradient terms.

Figure 1 shows TF densities for a void of $R = 20$ a.u. in an $r_s = 2$ a.u. metal, and the double-step model (DSM) density (dots) of Ref. 13. The solid line corresponds to the present ITFW model using $\beta = \frac{2}{9}$. The dashed-dotted line has been obtained using $\beta = \frac{1}{9}$. The agreement between the ITFW ($\beta = \frac{2}{9}$) density and that of Ref. 13 is reasonably good, indicating the reliability of our semiclassical model.

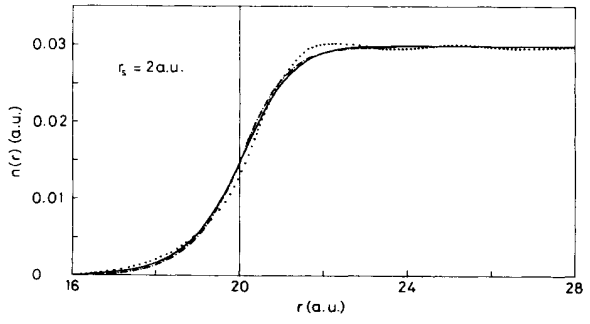

FIG. 1. ITFW densities for a void of $R = 20$ a.u. in an $r_s = 2$ a.u. metal using $\beta = \frac{2}{9}$ (solid line) and $\beta = \frac{1}{9}$ (dashed-dotted line) and the corresponding double-step model density of Ref. 13 (dots). The vertical line indicates the position of the jellium surface.

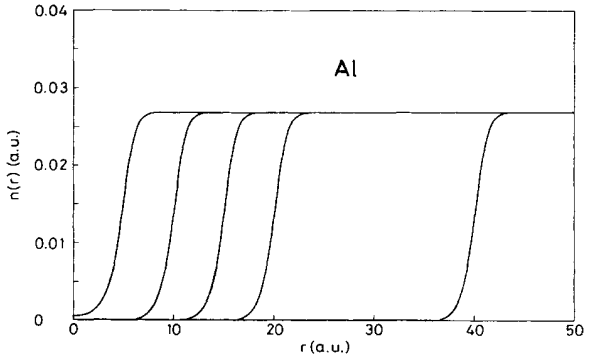

FIG. 2. ITFW densities for voids of R=5, 10, 15, 20, and 40 a.u. in Al ($r_s = 2.07$ a.u.).

Figure 2 displays the ITFW densities for Al ($r_s = 2.07$ a.u.) corresponding to voids of $R = 5$, 10, 15, 20, and 40 a.u. It is interesting to notice that for $R \gtrsim 15$ a.u., the electron-density profiles are basically parallel. This suggests that one can describe the electronic density of these voids by a universal function depending on a few parameters. We have checked that for voids of $R \gtrsim 15$ a.u., the variational densities can be represented by the function

$$n(r) = n_0 \left(1 - \frac{1}{\left[1 + \exp\left(\dfrac{r-(R+\delta)}{a}\right)\right]^\nu}\right) \ , \tag{27}$$

where the parameter δ takes into account that the derivative of the variational electron density is peaked inside the metal. The values $\nu = 1.801$, $\delta = 0.612$ a.u., and $a = 0.762$ a.u. reproduce quite well the variational results for Al down to $R \sim 10$ a.u.

Finally, we show in Fig. 3 the electron densities corresponding to $\epsilon_1 = \epsilon_2 = 1$ (dashed line), and to $\epsilon_1 = 3$,

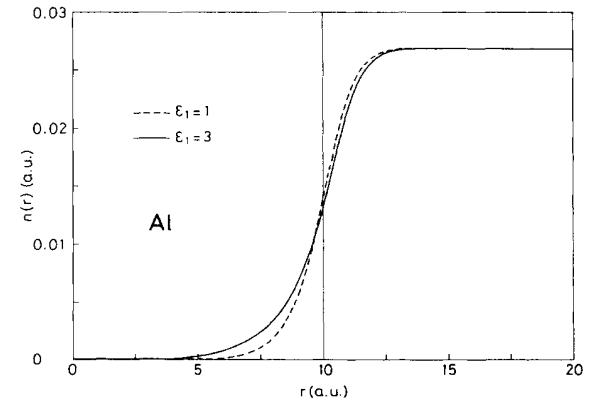

FIG. 3. ITFW electron densities corresponding to $\epsilon_1 = \epsilon_2 = 1$ (dashed line), and to $\epsilon_1 = 3$, $\epsilon_2 = 1$ (solid line) for a cavity of $R = 10$ a.u. in Al. The vertical line indicates the position of the jellium surface.

$\epsilon_2 = 1$ (solid line) for a cavity of $R = 10$ a.u. in Al. As we have previously indicated, because of the screening of the *e*-*e* interaction caused by the dielectric, the electron density "spills-in" the cavity, increasing the surface diffuseness.

B. The static polarizability of a void

For the sake of completeness, we use the ITFW method to work out the m_{-1} SR which is closely related to the static polarizability. We shall limit ourselves to the simpler case of a void, but with some obvious modifications the method can also be employed for bubbles.

Our method to obtain m_{-1} is described in great detail in Ref. 26. One has to solve the constrained problem

$$E[n] = \int d^3r\, \varepsilon[n] + \lambda \int d^3r\, Q(\mathbf{r})\, n(r)\ , \tag{28}$$

where in the present case $Q(\mathbf{r}) = r^{-(L+1)}Y_{L0}$ and λ is a small parameter. The corresponding EL equation

$$\frac{\delta\varepsilon[n]}{\delta n} + \lambda \frac{1}{r^{L+1}} Y_{L0} = \mu \tag{29}$$

is solved to first order in λ by using as electron density

$$n(\mathbf{r}) \equiv n_e(r) + \delta n(\mathbf{r}) \equiv n_e(r) + \lambda f(r)\, Y_{L0}\ , \tag{30}$$

where $n_e(r)$ is the ITFW equilibrium density obtained when $\lambda = 0$. The unknown function $f(r)$ obeys the following integro-differential equation:

$$-\frac{\beta}{4}\frac{d^2f}{dr^2} + \frac{\beta}{4}\left(-\frac{2}{r} + \frac{n_e'}{n_e}\right)\frac{df}{dr} + \left\{\frac{\beta}{4}\left[\frac{L(L+1)}{r^2} + \frac{\Delta n_e}{n_e} - \left(\frac{n_e'}{n_e}\right)^2\right] + \tfrac{5}{9}\gamma n_e^{2/3} - \tfrac{4}{9}c_x n_e^{1/3} - \tfrac{2}{9}a\, r_s(n_e)\frac{b + 2r_s(n_e)}{[b + r_s(n_e)]^3}\right\} f$$

$$+ n_e \frac{1}{r^{L+1}} + \frac{4\pi}{2L+1}\left[\frac{n_e}{r^{L+1}}\int_0^r dr_1\, r_1^{L+2} f(r_1) + n_e\, r^L \int_r^\infty dr_1 \frac{f(r_1)}{r_1^{L-1}}\right] = 0\ . \tag{31}$$

In this equation, n_e' and Δn_e denote, respectively, the r derivative and the Laplacian of the g.s. equilibrium density, and $r_s(n_e) = (4\pi n_e/3)^{-1/3}$ is the *local* radius per electron. The constants have been defined in Eqs. (6), (7), and (23). Once Eq. (31) has been solved, the static polarizability α is readily obtained,[26]

$$\alpha = 2\, m_{-1} = -\int_0^\infty dr\, f(r)\, r^{-(L-1)}\ . \tag{32}$$

It is worth noting that the term multiplied by $4\pi/(2L+1)$ in Eq. (31) comes from the *e*-*e* Coulomb direct potential. This is the only term that should be modified in the case of a bubble, using the results given in the Appendix. The differential character of Eq. (31) comes from the Weizsäcker term in Eq. (23). Otherwise, one deals with a simpler integral equation.

It is interesting to work out in detail the classical limit obtained when only the Coulomb term is kept in Eq. (31). The resulting integral equation

$$\frac{1}{R^{L+1}} + \frac{4\pi}{2L+1}\left[\frac{1}{R^{L+1}}\int_0^R dr\, r^{L+2} f(r) + R^L \int_R^\infty dr\, \frac{f(r)}{r^{L-1}}\right] = 0 \tag{33}$$

has a solution of the type $f(r) = c\,\delta(r - R)$, as can be checked substituting this expression into Eq. (33). One easily finds

$$c = -\frac{2L+1}{4\pi}\frac{1}{R^{L+2}}\ .$$

Thus,

$$m_{-1} = \tfrac{1}{2}\alpha_{\rm cl} = \frac{2L+1}{8\pi}\frac{1}{R^{2L+1}}\ . \tag{34}$$

Using Eqs. (14) and (34), one gets for the classical frequency

$$E_1^2 = \frac{m_1}{m_{-1}} = 4\pi n_0 \frac{L+1}{2L+1} = \omega_p^2 \frac{L+1}{2L+1} = \omega_{\rm cl}^2\ . \tag{35}$$

Equations (17) and (35) show that in the classical limit $E_1 = E_3$, meaning that for a given L there is a single plasmon mode which has no spatial dispersion (i.e., its energy does not depend on the radius of the void). The radius dependence comes from the quantal kinetic energy and from the surface diffuseness, which is also a quantum effect.

Figure 4 shows the dipole "induced density" $f(r)$ for two typical Al voids of $R = 10$ and 30 a.u. obtained from the full solution of Eq. (31) (solid lines, left scale), and from the solution of the integral equation that results in putting $\beta = 0$ in that equation and using a constant electronic density n_0 (dashed lines, right scale). The function $f(r)$ has been normalized as follows:

$$\int_0^\infty dr\, r^2\, f(r) = 1\ .$$

For the ITFW model, $f(r)$ is located well inside the void, at variance with the result of the unrealistic step density (SD) model. This spill-in of the induced density caused

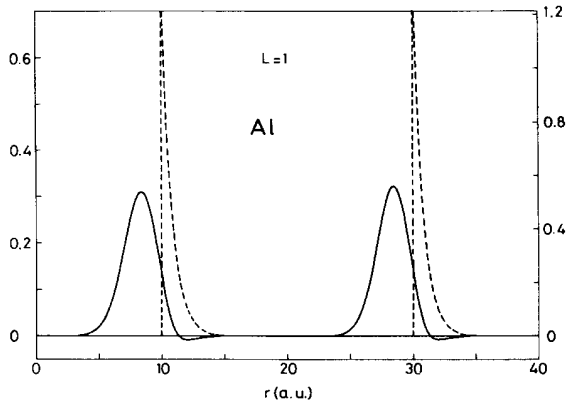

FIG. 4. Normalized dipole induced densities $f(r)$ for two voids of $R = 10$ and 30 a.u. in Al obtained from the full (solid lines, left scale) and the $\beta = 0$, constant electron-density (dashed lines, right scale) solutions of Eq. (31).

by the electronic surface diffuseness has a dramatic effect on the value of the static polarizability. This can be seen from Fig. 5, which shows the static dipole polarizability in units of $\alpha_{\rm cl}$, Eq. (34). The solid line corresponds to the ITFW model and the dashed line to the SD model, which fails to yield the qualitative behavior of $\alpha/\alpha_{\rm cl}$ as a function of R. A similar situation was found in NFE metal spheres some time ago,[25,26,32] and only the use of realistic electronic densities in the calculations yielded a semiquantitative reproduction of the experimental results.[33]

To avoid any possible misunderstanding, we want to emphasize that Eqs. (8), (10), (12), and (20) are exact RPA expressions, provided they are evaluated using the corresponding KS densities. The use in Sec. IV of the ITFW model to evaluate these equations is just a matter of convenience justified by the fact that SR calculations for metal spheres in the KS and ITFW approximations yield results in excellent agreement with each other (see Refs. 26, 19, and 34). In contradistinction, Eq. (32) is not a RPA result. However, it has been shown in different situations that Thomas-Fermi models of similar complexity as the one used here yield a static polarizability

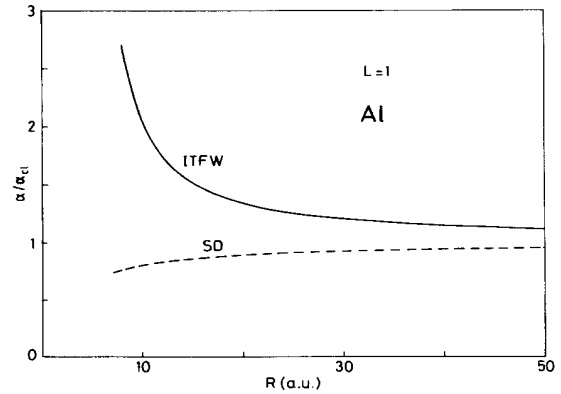

FIG. 5. Static dipole polarizability in units of the classical value, Eq. (34), in the ITFW (solid line) and SD (dashed line) models, as a function of R.

in good agreement with the exact RPA result. We refer the reader to Refs. 17, 21, 34, and 35 for a discussion of this point.

IV. NUMERICAL RESULTS FOR THE SURFACE-PLASMON ENERGY

Before presenting the numerical results, we would like to say a word of caution about the singularity of the operator $Q(\mathbf{r}) = r^{-(L+1)}Y_{L0}$ that generates the surface oscillations. We have explicitly assumed in the derivation of Eqs. (8), (10), (12), and (20) that $n(r)$ is zero at the origin. Actually, one can see from these formulas that for them to be valid, $n(r)$ must go to zero faster than some power of r which increases with increasing L. In practice, we have limited ourselves to cavities with $R \gtrsim 5$ a.u., for which the surface, defined as the region where the density changes from 10% to 90% of the bulk value n_0, is well apart from the origin, and have introduced an effective density

$$n_{\rm eff}(r) = \theta(r - R_{\rm cut})\, n(r) \ ,$$

with the requirement that the surface region of the variational $n(r)$ is fully incorporated into $n_{\rm eff}(r)$. For the results we shall be describing, we have checked that the value of the cutoff radius $R_{\rm cut}$ can be taken rather arbitrarily without appreciably changing the numerical results. When, due to the chosen values of R and/or L, it has not been the case, we have stopped the calculation since it is no longer reliable.

The integrals over $r^{-(2L+2)}$ in Eqs. (8), (10), and (20) and, to a lesser extent, the one over $r^{-(2L+4)}$ in Eq. (12), must be carried out with some care. They are slowly converging and stopping their evaluation at the R_∞ value defined in Sec. III A, which is perfectly valid for the structure calculation, can cause numerical inaccuracies, especially for large voids. Since at R_∞ the functions $n(r)$ and $\tau(r)$ have reached their asymptotic values n_0 and τ_0, we have added to the computed integral the corresponding rest calculated as in the SD model. In the case of Eq. (8), for example, we have added to the integral

$$\int_0^{R_\infty} dr\, \frac{n(r)}{r^{2L+2}}$$

the value

$$\frac{n_0}{2L+1}\,\frac{1}{R_\infty^{2L+1}} \ ,$$

which results from analytically evaluating that integral from R_∞ to infinity.

The results we shall discuss correspond to Al ($r_s = 2.07$ a.u.). We have chosen this typical NFE metal for all the numerical calculations presented in this work (except Fig. 1) because of the available experimental data on bubbles in aluminum.

A. Voids

We present in Fig. 6 the E_3 energy for $L = 1$ and $\epsilon_1 = \epsilon_2 = 1$ obtained from models of different complexity.

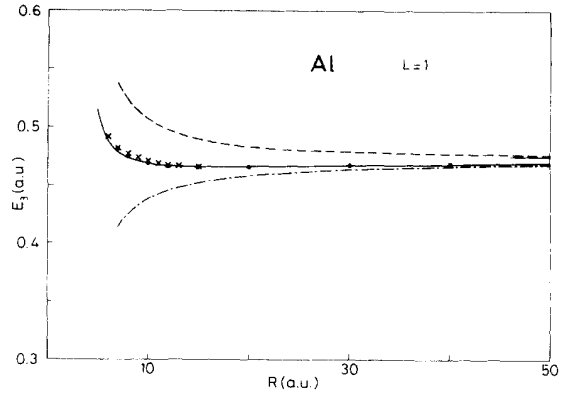

FIG. 6. Average $L = 1$ E_3 energy as a function of R for voids ($\epsilon_1 = \epsilon_2 = 1$). Solid line: complete ITFW calculation with $\beta = \frac{2}{9}$. The crosses correspond to $\beta = \frac{1}{9}$. Dashed line: step electron density model. Dashed-dotted line: neglecting the kinetic contribution to E_3. The dots along the E_3 solid curve have been obtained using the electronic density defined in Eq. (27). The horizontal line at the right-hand side is the classical limit.

The dashed line corresponds to the SD result, and the dots to the E_3 energies obtained using the parametrized electron densities, Eq. (27). The solid line shows the complete ITFW calculation with $\beta = \frac{2}{9}$. As a test of the sensitivity of our results to the parameter β we also include the results for $\beta = \frac{1}{9}$ (crosses).

Another hint about the sensitivity of the results to the value of β used in Eq. (23), as well as the adequacy of the value here adopted, is furnished by Table I. In this table, the results labeled as DSM have been obtained using in Eqs. (8), (10), (12), and (23) (with $\beta = \frac{2}{9}$), the DSM densities for R=7, 14, and 20 a.u. We would like to indicate that these DSM densities have been obtained digitalizing the results displayed in Figs. 1(a) and 2(a) of Ref. 13. One can see that the agreement between the TF and DSM results is good. However, one should have in mind that we have assumed the same kinetic-energy functional in both cases.

We see from Fig. 6 that the energy of the surface excitation goes to the classical limit (indicated by a horizontal line at the right side) when R increases, due to the dominant role played by the Coulomb term. For voids of small radius, the energy is mainly determined by the kinetic-energy contribution, and thus it sharply increases below $R \sim 10$ a.u. The smooth minimum around $R \sim 15$ a.u. is due to the interplay between the kinetic-energy and surface diffuseness effects which are absent in the SD model. Indeed, if we neglect the kinetic contribution to E_3 and consider the Coulomb potential as the only source of the restoring force of the mode, we obtain the dashed-dotted line, which shows a size dependence coming from the surface diffuseness. In the complete calculation, this effect is compensated by the kinetic contribution when the radius is small enough. The similarity between the result of the complete calculation (solid line) and that of Aers, Paranjape, and Boardman[11] obtained from a hydrodynamical model is remarkable.

The dominance of the kinetic-energy contribution at small radii is a consequence of the strong localization of the induced charge. For very small voids, the excitation loses its collective character degenerating into an electron-hole pair (incidentally, this makes less restrictive the fact that the method cannot be applied to small voids for the reasons discussed at the beginning of this section). At small distances, the electron-hole pair compensates with an equally strong kinetic-energy amount, the strong negative potential energy needed to make a dipole. We thus conclude that the blueshift of ω with respect to the classical value $\omega_{\rm cl}$ for small radii is a kinetic-energy effect.

The angular-momentum dependence of the plasmon energy can be seen in Fig. 7, where we have plotted $E_3(L)$ versus R for $L = 1$ to 3. Also indicated at the right-hand side by horizontal lines are the $L = 1$ and 3 classical values. As expected from the higher power of L appearing in $m_3(T)$ than in $m_3(C)$ [see Eqs. (15) and (16)], for large L values and a given R, the kinetic contribution is taking over the Coulomb one farther away from the origin, displacing the smooth minimum of the curves towards larger radii. As a consequence, the minimum is swept up because of the minor role played by the surface diffuseness when R increases.

For a given R, the collective character of the L mode is being washed out as L increases. If, for a given

TABLE I. Plasmon energies for voids of R=7, 14, and 20 a.u. in an $r_s = 2$ a.u. metal for L=1 and 2. The results labeled WB have been taken from Ref. 13. The DSM results are E_3 energies obtained using the densities given in Ref. 13. The other results have been obtained using different values of the parameter β in Eq. (23).

R	L	WB	DSM	$\beta = \frac{1}{9}$	$\beta = \frac{2}{9}$
7	1	0.541	0.501	0.507	0.502
	2	0.537	0.511	0.514	0.511
14	1	0.520	0.489	0.492	0.490
	2	0.505	0.466	0.472	0.469
20	1	0.512	0.491	0.492	0.490
	2	0.497	0.464	0.466	0.464

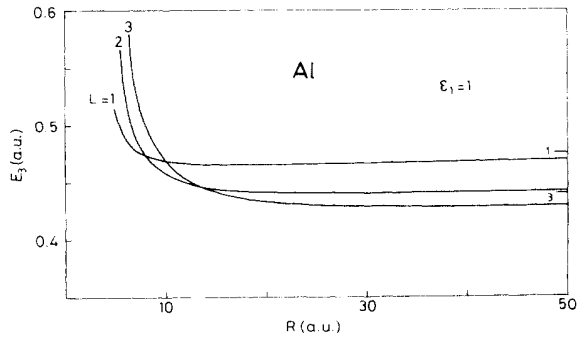

FIG. 7. $E_3(L)$ vs R for $L = 1$ to 3. The horizontal lines at the right-hand side are the classical $L = 1$ and 3 values, Eq. (1).

angular momentum, we take as a rough criterion of collectivity losing the equality of kinetic and Coulomb contributions,[18] we obtain from Eqs. (15) and (16) the following estimate of the minimum radius $R_{\min}$ of the void that can sustain a collective L mode:

$$R_{\min} = (2L+1)\sqrt{\frac{2(L+2)}{3(L+1)}}\frac{\beta_F}{\omega_p} . \quad (36)$$

This gives for Al a radius of about 4 a.u. for $L = 1$, and 8 a.u. for $L = 3$. A similar formula can be worked out for bubbles using Eqs. (16) and (21).

B. Bubbles

To estimate the changes introduced by the dielectric in the frequency of the surface plasmon, we first considered the case in which $\epsilon_1 = 3$, $\epsilon_2 = 1$. The effect of the dielectric on the g.s. electronic density has been described in Sec. III A, Fig. 3.

Figure 8 shows the average dipole E_3 energy as a function of R (solid line). For comparison, we show again the results corresponding to $\epsilon_1 = \epsilon_2 = 1$ (dashed line). The general trends of $E_3(R)$ can be easily understood from the analysis we have carried out in the case of voids. Notice that in the present case, and for sizes bigger than $R \sim 10$ a.u., E_3 is increasing with R. This is due to the increase of the electronic diffuseness and spill-in, whose effect now takes over the kinetic energy one for sizes smaller than in the $\epsilon_1 = 1$ case. However, we do not calculate E_3 for smaller bubbles ($R < 7$ a.u.) because of the requirements explained at the beginning of Sec. IV.

It is worth noting the sizable shift of $E_3(R)$ with respect to the $\epsilon_1 = 1$ case. This effect is essentially due to the explicit appearance of the dielectric constant in Eq. (20). To show it, we have evaluated Eq. (20) using the $\epsilon_1 = \epsilon_2 = 1$ self-consistent densities. In this case, we get for $E_3(R)$ the dashed-dotted line in Fig. 8. The difference between the solid and dashed-dotted lines is the effect of the dielectric through self-consistently changing the electronic densities. The disappearance of the minimum when we use the $\epsilon_1 = \epsilon_2 = 1$ electronic densities is again a diffuseness effect: these densities lack the appropriate diffuseness to give rise to the minimum shown by the exact calculation.

We have also checked that the last three terms in Eq. (20), which are strictly zero in the SD model, contribute very little to $m_3(C)$ when the density is diffuse. In the case under study, these last three terms amount to a negligible 0.4% of the total $m_3(C)$ for $R = 40$ a.u., a 2.5% for $R = 20$ a.u., and a 7% for $R = 10$ a.u., an R value for which m_3 already gets an appreciable contribution from the kinetic energy.

Figure 9 shows the average energy of the dipole surface plasmon for different values of the dielectric constant in the cavity (ϵ_1) and $\epsilon_2 = 1$. The circles on that figure correspond to experimental data on bubbles of Ne, Ar, and Xe in aluminum.[3,12] For the first two gases, it was experimentally possible to obtain information about the density of the gas inside the bubble, the bubble radius, and the surface-plasmon energy. To obtain ϵ_1 and thus be able to compare with the results of our calculations, we have used the experimental atomic polarizabilities [$\alpha(\text{Ne}) = 0.39 \times 10^{-24}$ cm^3, $\alpha(\text{Ar}) = 1.62 \times 10^{-24}$ cm^3, and $\alpha(\text{Xe}) = 3.99 \times 10^{-24}$ cm^3] in the Clausius-Mossotti formula. In the first two cases, the difference between experimental and calculated results is about 1% for Ne and 6% for Ar [when making the comparison, notice that $\epsilon(\text{Ne}) = 1.41$ and $\epsilon(\text{Ar}) = 2.12$]. In the third case, there is a coupling effect between the surface-plasmon and the $^1S_0$-$^1P_1$ inner electronic excitation of Xe, which prevents the experimental determination of the plasmon energy. Nonetheless, if one uses the measured radius and the experimental dielectric constant to locate the Xe point on the figure [$\epsilon(\text{Xe}) = 2.87$], the resulting frequency $\omega = 0.365$ a.u. agrees well with the expected one.

We have also plotted in Fig. 9 a set of experimental

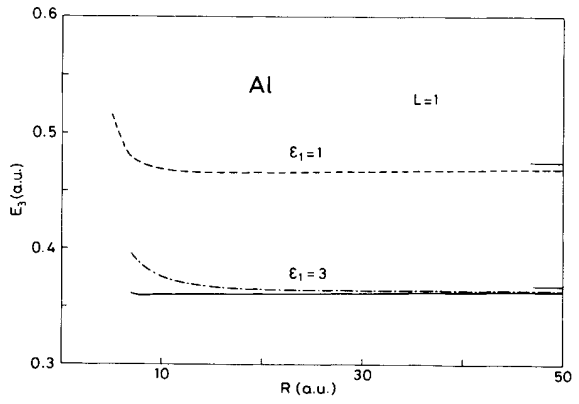

FIG. 8. Dipole E_3 energy as a function of R. Solid line: bubbles with $\epsilon_1 = 3$ and $\epsilon_2 = 1$. Dashed line: voids ($\epsilon_1 = \epsilon_2 = 1$). Dashed-dotted line: using the $\epsilon_1 = \epsilon_2 = 1$ densities in the $\epsilon_1 = 3, \epsilon_2 = 1$ formulas. The horizontal lines at the right-hand side are the classical values obtained from the Coulomb contribution in Eq. (22).

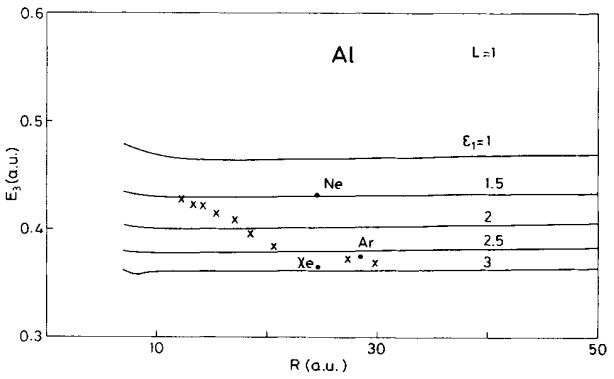

FIG. 9. Average energy of the dipole surface plasmon for different values of the dielectric constant in the cavity and $\epsilon_2 = 1$. Circles: experimental data for bubbles of Ne ($\epsilon_1 = 1.41$), Ar ($\epsilon_1 = 2.12$), and Xe ($\epsilon_1 = 2.87$) in Al. Crosses: experimental data for He bubbles in Al. From left to right, the crosses correspond to bubbles of $\epsilon_1 = 1.42, 1.41, 1.39, 1.37, 1.36, 1.33, 1.31, 1.24$, and 1.19, respectively.

data (crosses) taken from He bubbles in Al,[12] placing them on the figure using the relationships between the concentration, radius, and density given in Ref. 13. These data seem to indicate that the gas density in the bubble decreases as the bubble radius increases, thus leading to a decrease of the dielectric constant. Our model does not reproduce these data, although one should have in mind the rather large width (about 12 a.u.) of the experimental size distribution.[12] Manzke, Crecelius, and Fink[12] have suggested that their experimental results can be explained by a bubble-bubble interaction. Indeed, when the gas dose is big enough, the density of bubbles increases and their mutual interaction makes them crystallize. This causes the single L modes of the isolated bubbles to merge into continuous bands with predictable quite different properties.

Lucas[7] has shown that most of the bubble-bubble interaction comes from its monopolar $L = 0$ component, which is much stronger than the van der Waals force responsible for the mutual attraction between metallic spheres. This mode is not the $L = 0$ multipole corresponding to our ansatz, Eq. (5), as this one generates a charge fluctuation[19]

$$n_1^{L=0}(r) = -\nabla(n\nabla Q) = Y_{00}\frac{1}{r^2}\frac{dn}{dr} \tag{37}$$

which, integrated over the whole space, is not zero. The $L = 0$ is a volume mode that can be generated by the q- and L-dependent operator[36]

$$Q'(\mathbf{r}) = y_L(qr)Y_{L0} , \tag{38}$$

where $y_L(qr)$ is a spherical Bessel function of the second kind,[37] and that for $L = 0$ and (qr) going to zero behaves as $Y_{00}/(qr)$. The integral of the induced density $n_1^{L=0}(r)$ associated with Q' is zero as a consequence of the oscillatory nature of Q', and the energy of this mode tends to ω_p for big radii. Following the method of Ref. 19, it can be shown that in the step density approximation the Coulomb term contributes to the monopole energy, but not the kinetic term.

V. CONCLUDING REMARKS

In this work we have studied the electronic surface modes of cavities in metals within a RPA sum-rules approach. The static dipole polarizability of voids has also been investigated, and the nature of the $L = 0$ mode, which is relevant for the process of bubble crystallization,[7] has been briefly discussed.

The behavior of the plasmon energy as a function of the radius of the cavity has been studied with some detail, disentangling the electronic kinetic- and Coulomb energy contributions, as well as the effect of the surface diffuseness. For the step density model we have obtained a simple formula, Eq. (22), that could be useful in applications of the model to spectroscopic calculations.

In the case of bubbles, we have included the dielectric properties of the gas inside the cavity, not only through the electronic density, but also explicitly in the electronic response. We have shown that this latter effect is by far the most important one. It has been systematically neglected in the description of the surface response of bubbles[13] and metal spheres embedded in a dielectric.[28] The formulas we have deduced for the surface energy allow one to incorporate the effect of the ionic cores whenever it can be modeled by a constant dielectric function, as indicated in Ref. 21. However, in the numerical applications presented here we have not exploited this possibility.

Although the SR approach yields only average energy values, we hope to have shown in this paper, and in the previous ones about metal spheres, that the method is a very powerful and simple one to investigate the general features of collective modes of NFE metals. Indeed, very often it allows us to obtain a deeper physical insight than a detailed evaluation of the strength function, as it yields formulas that can be easily interpreted in terms of the different terms (kinetic, Coulomb, exchange, etc.) of the energy density functional.

ACKNOWLEDGMENTS

We are indebted to Ángel Rubio for interesting discussions. This work has been supported by the DGICYT (Spain) under Grants Nos. PB89/332, PB88/069, and BE89/019, by the CIRIT (Catalonia), and by the Universitat de Barcelona–Universitat de les Illes Balears and Universitat de València–Universitat de les Illes Balears exchange programs.

APPENDIX

The general expression for the scalar Coulomb potential $\Phi(\mathbf{r}_1, \mathbf{r}_2)$ created by an elementary charge at $\mathbf{r}_1$, in a point $\mathbf{r}_2$ of a space occupied by a spherical dielectric of radius R and constant ϵ_1 surrounded by an infinite dielectric of constant ϵ_2, reads

$$\Phi(\mathbf{r}_1,\mathbf{r}_2) = \begin{cases} \displaystyle\sum_l \left[\frac{A_l}{r_2^{l+1}} + \frac{r_<^l}{\epsilon_2\, r_>^{l+1}}\right] P_l(\cos\theta) & \text{if } r_1, r_2 > R \\ \displaystyle\sum_l B_l\, r_2^l\, P_l(\cos\theta) & \text{if } r_1 > R,\ r_2 < R \\ \displaystyle\sum_l \frac{C_l}{r_2^{l+1}}\, P_l(\cos\theta) & \text{if } r_1 < R,\ r_2 > R \\ \displaystyle\sum_l \left[D_l\, r_2^l + \frac{r_<^l}{\epsilon_1\, r_>^{l+1}}\right] P_l(\cos\theta) & \text{if } r_1, r_2 < R , \end{cases} \tag{A1}$$

where θ is the angle formed by the vectors $\mathbf{r}_1$ and $\mathbf{r}_2$. The constants A_l, B_l, C_l, and D_l are obtained imposing the continuity of the potential and of the normal component of the displacement vector at R. This yields

$$\Phi(\mathbf{r}_1,\mathbf{r}_2)=\begin{cases}\dfrac{4\pi}{\epsilon_2}\displaystyle\sum_{lm}\dfrac{1}{2l+1}\left[\dfrac{r_<^l}{r_>^{l+1}}+\dfrac{R^{2l+1}}{r_1^{l+1}r_2^{l+1}}\dfrac{l(\epsilon_2-\epsilon_1)}{\epsilon_1 l+\epsilon_2(l+1)}\right]Y_{lm}^*(\Omega_1)\,Y_{lm}(\Omega_2) & \text{if } r_1,r_2>R\\ 4\pi\displaystyle\sum_{lm}\dfrac{r_2^l}{r_1^{l+1}}\dfrac{Y_{lm}^*(\Omega_1)\,Y_{lm}(\Omega_2)}{\epsilon_1 l+\epsilon_2(l+1)} & \text{if } r_1>R,\ r_2<R\\ 4\pi\displaystyle\sum_{lm}\dfrac{r_1^l}{r_2^{l+1}}\dfrac{Y_{lm}^*(\Omega_1)\,Y_{lm}(\Omega_2)}{\epsilon_1 l+\epsilon_2(l+1)} & \text{if } r_1<R,\ r_2>R\\ \dfrac{4\pi}{\epsilon_1}\displaystyle\sum_{lm}\dfrac{1}{2l+1}\left[\dfrac{r_<^l}{r_>^{l+1}}+\dfrac{r_1^l r_2^l}{R^{2l+1}}\dfrac{(l+1)(\epsilon_1-\epsilon_2)}{\epsilon_1 l+\epsilon_2(l+1)}\right]Y_{lm}^*(\Omega_1)\,Y_{lm}(\Omega_2) & \text{if } r_1,r_2<R.\end{cases}\tag{A2}$$

[1] S. F. Pugh, M. H. Loretto, and D. I. R. Norris, in *Proceedings of the European Conference on Voids Formed by Irradiation of Reactor Materials* (British Nuclear Energy Society, Reading, England, 1971), p. IV.

[2] J. von den Driesch and P. Jung, High Temp. High Pressures **12**, 635 (1980).

[3] A. vom Felde, J. Fink, Th. Müller-Heinzerling, J. Pflüger, B. Scheerer, G. Linker, and D. Kaletta, Phys. Rev. Lett. **53**, 922 (1984).

[4] P. Henoc and L. Henry, J. Phys. (Paris) Colloq. Suppl. 4, **31**, C1-55 (1970).

[5] M. Natta, Solid State Commun. **7**, 823 (1969).

[6] R. H. Ritchie and R. E. Willems, Phys. Rev. **178**, 372 (1969).

[7] A. A. Lucas, Phys. Rev. B **7**, 3527 (1976).

[8] J. C. Ashley and T. L. Ferrell, Phys. Rev. B **14**, 3277 (1973).

[9] R. M. Nieminen, Phys. Status Solidi B **66**, 183 (1974).

[10] V. V. Maksimenko, A. J. Simonov, and A. A. Lushnikov, Phys. Status Solidi B **82**, 685 (1977).

[11] G. C. Aers, B. V. Paranjape, and A. D. Boardman, J. Phys. Chem. Solids **40**, 319 (1979).

[12] R. Manzke, G. Crecelius, and J. Fink, Phys. Rev. Lett. **51**, 1095 (1983).

[13] K. D. Wu and D. E. Beck, Phys. Rev. B **36**, 998 (1987).

[14] J. C. Rife, S. E. Donnelly, A. A. Lucas, J. M. Gilles, and J. J. Ritsko, Phys. Rev. Lett. **46**, 1220 (1981).

[15] A. A. Lushnikov and A. J. Simonov, Z. Phys. **270**, 17 (1974).

[16] G. Bertsch and W. Ekardt, Phys. Rev. B **32**, 7659 (1985).

[17] M. Brack, Phys. Rev. B **39**, 3533 (1989).

[18] Ll. Serra, F. Garcias, M. Barranco, J. Navarro, L. C. Balbás, and A. Mañanes, Phys. Rev. B **39**, 8247 (1989).

[19] Ll. Serra, F. Garcias, M. Barranco, N. Barberán, and J. Navarro, Phys. Rev. B **41**, 3434 (1990).

[20] E. Lipparini and S. Stringari, Z. Phys. D **18**, 193 (1991).

[21] Ll. Serra, F. Garcias, M. Barranco, N. Barberán, and J. Navarro, Phys. Rev. B **44**, 1492 (1991).

[22] P. Gleissl, M. Brack, J. Meyer, and Ph. Quentin, Ann. Phys. (N.Y.) **197**, 205 (1990).

[23] C. Yannouleas, R. A. Broglia, M. Brack, and P. F. Bortignon, Phys. Rev. Lett. **63**, 255 (1989).

[24] R. S. Sorbello, Solid State Commun. **48**, 989 (1983).

[25] W. Ekardt, Phys. Rev. Lett. **52**, 1925 (1984).

[26] Ll. Serra, F. Garcias, M. Barranco, J. Navarro, L. C. Balbás, A. Rubio, and A. Mañanes, J. Phys. Condens. Matter **1**, 10391 (1989).

[27] A. Rubio, L. C. Balbás, Ll. Serra, and M. Barranco, Phys. Rev. B **42**, 10950 (1990).

[28] M. J. Puska, R. M. Nieminen, and M. Manninen, Phys. Rev. B **31**, 3486 (1985).

[29] M. Manninen, R. Nieminen, P. Hautojärvi, and J. Arponen, Phys. Rev. B **12**, 4012 (1975).

[30] D. Kirzhnits, *Field Theoretical Methods in Many Body Systems* (Pergamon, Oxford, 1967).

[31] M. Centelles, M. Pi, X. Viñas, F. Garcias, and M. Barranco, Nucl. Phys. **A510**, 397 (1990).

[32] D. R. Snider and R. S. Sorbello, Phys. Rev. B **28**, 5702 (1983).

[33] W. A. de Heer, W. D. Knight, M. Y. Chou, and M. L. Cohen, in *Solid State Physics*, edited by H. Ehrenreich, F. Seitz, and D. Turnbull (Academic, Orlando, 1987), Vol. 40, p. 93.

[34] Ll. Serra, F. Garcias, N. Barberán, M. Barranco, J. Navarro, and A. Rubio, Z. Phys. D **19**, 89 (1991).

[35] E. Lipparini and S. Stringari, Phys. Rep. **175**, 103 (1989).

[36] N. Barberán and J. Bausells, Solid State Commun. **73**, 651 (1990).

[37] *Handbook of Mathematical Functions*, edited by M. Abramowitz and I. A. Stegun (Dover, New York, 1970), Chap. 10.